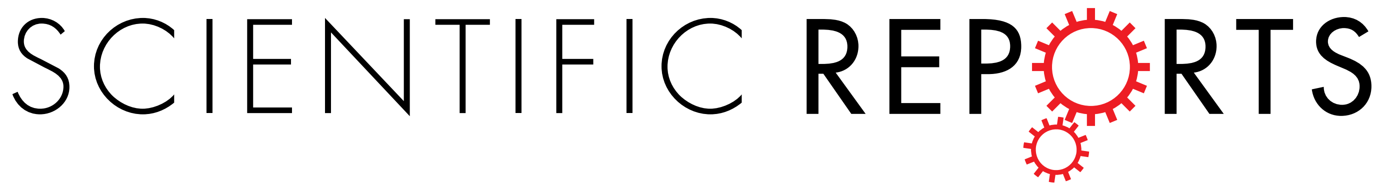

OPEN

Enhancement of the Si *p-n* diode NIR photoresponse by embedding β-$FeSi_2$ nanocrystallites

Received: 10 December 2014
Accepted: 09 September 2015
Published: 05 October 2015

A.V. Shevlyagin[1], D.L. Goroshko[1,2], E.A. Chusovitin[1], K.N. Galkin[1,2], N.G. Galkin[1,2] & A.K. Gutakovskii[3,4]

By using solid phase epitaxy of thin Fe films and molecular beam epitaxy of Si, a p^+-Si/*p*-Si/β-$FeSi_2$ nanocrystallites/*n*-Si(111) diode structure was fabricated. Transmission electron microscopy data confirmed a well-defined multilayered structure with embedded nanocrystallites of two typical sizes: 3–4 and 15–20 nm, and almost coherent epitaxy of the nanocrystallites with the Si matrix. The diode at zero bias conditions exhibited a current responsivity of 1.7 mA/W, an external quantum efficiency of about 0.2%, and a specific detectivity of 1.2×10^9 cm $\times$ $Hz^{1/2}$/W at a wavelength of 1300 nm at room temperature. In the avalanche mode, the responsivity reached up to 20 mA/W (2% in terms of efficiency) with a value of avalanche gain equal to 5. The data obtained indicate that embedding of β-$FeSi_2$ nanocrystallites into the depletion region of the Si *p-n* junction results in expansion of the spectral sensitivity up to 1600 nm and an increase of the photoresponse by more than two orders of magnitude in comparison with a conventional Si *p-n* junction. Thereby, fabricated structure combines advantage of the silicon photodiode functionality and simplicity with near infrared light detection capability of β-$FeSi_2$.

Light detection in the near-infrared region (NIR), especially at the telecommunication wavelengths (1300 and 1550 nm), is an important issue for optical fibre communication systems because of the low dispersion and low loss characteristics of the silica fibres[1]. To step into the future of integrated optoelectronics, we need light sources and detectors that are compatible with conventional Si technology. That is why, despite the success of applications of, for example, $A_{III}B_V$-based photodetection materials, such as InAs/GaSb/AlSb superlattices[2,3], their utilization is limited. On the other hand, in recent years there has been considerable progress in terms of the development of photodetecting structures on Si substrates. Among them are other group IV materials and their alloys, quantum dots, or wells, namely GeSn *p-i-n*[4,5] or SiGe structures[6–8], and graphene-based photodetectors grown on Si[9,10]. The common drawback of these structures is the absence of effective light sources based on the very same materials.

Therefore, the semiconducting iron disilicide (β-$FeSi_2$) has the advantage of the ability to simultaneously emit and detect light. Semiconducting iron disilicide exhibits a band gap of approximately 0.8 eV and a very large optical absorption coefficient of over $10^5\,cm^{-1}$ at 1 eV[11]. It was shown that the Si/β-$FeSi_2$ heterostructure diode possesses electroluminescence at a wavelength of 1550 nm at room temperature with an external quantum efficiency near to 0.1%[12]. Hence, the development of Si/β-$FeSi_2$ structures with sufficient photodetection properties in the NIR can open up the possibility of designing opto-couples and lead to advanced silicon optoelectronics. Moreover, β-$FeSi_2$ is compatible with the current Si technology, and both Fe and Si are abundant in the Earth's crust[13].

[1]Institute of Automation and Control Processes FEB RAS, Radio St. 5, 690041 Vladivostok, Russia. [2]Far Eastern Federal University, School of Natural Sciences, Sukhanova St. 8, 690950 Vladivostok, Russia. [3]Rzhanov Institute of Semiconductor Physics, SB RAS, Lavrentieva Ave.1, 630090 Novosibirsk, Russia. [4]Novosibirsk State University, Pirogova St. 2, 630090 Novosibirsk, Russia. Correspondence and requests for materials should be addressed to A.V.S. (email: shevliagin@mail.ru)

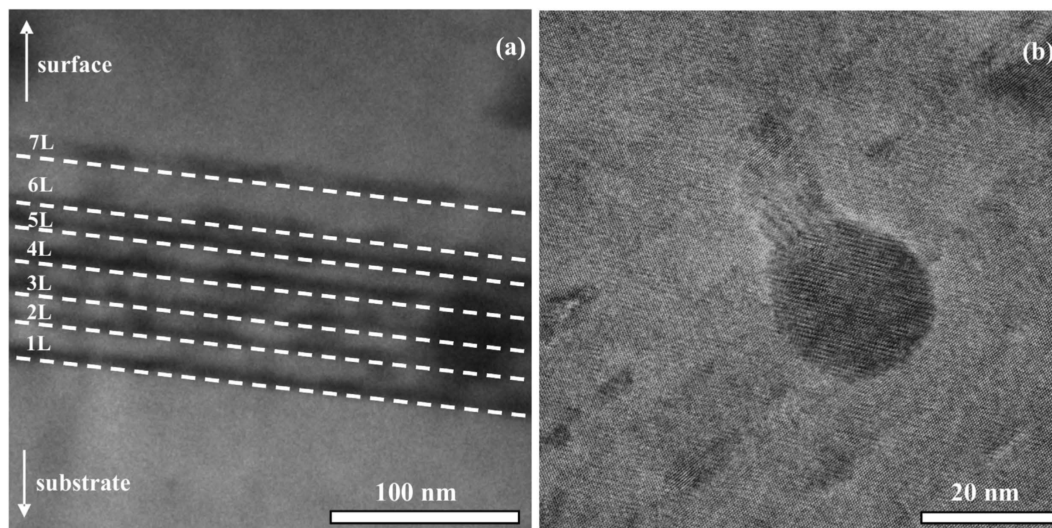

Figure 1. Cross-sectional TEM images of the seven-layered Si/β-FeSi$_2$ NCs/Si structure. (**a**) A general view. (**b**) HRTEM image indicating the presence of two types of β-FeSi$_2$ NCs. Dashed lines indicate the borders of the layers.

Unfortunately, most of the research teams emphasize that two main factors, associated with trap centres for photogenerated carriers, limit the performance of the Si/β-FeSi$_2$ photodiode structure. The first of these factors is the diffusion of iron atoms into the silicon substrate during β-FeSi$_2$ formation, which results in deep level formation[14], and the second is the existence of dangling bonds in the heterojunction interface and initial β-FeSi$_2$ layer, which causes the interface states[15]. In particular, the heterojunction interface between the β-FeSi$_2$ film and the Si substrate has dangling bonds due to both grain boundaries and a lattice mismatch[16].

In this work, we demonstrate an approach to spectral expansion of the silicon *p-n* junction photodetecting properties in the NIR by embedding β-FeSi$_2$ nanocrystallites (NCs) into a *p*-type silicon layer. To reduce iron diffusion into the substrate, the deposition of thin 0.4 nm Fe layers is performed at room temperature. A multilayered structure obtained in this way would contain at most several nanometres of Fe, while for the same photodetection performance on β-FeSi$_2$ films it is necessary to use hundreds of nanometres. In addition, heteroepitaxial stress may result in changes of the optical properties, band gap, and even electron dispersion law of the embedded β-FeSi$_2$[17]. It was shown that photovoltaic properties of Si/β-FeSi$_2$ film heterostructure are strongly limited by the diffusion length of the minority carriers in the β-FeSi$_2$ absorbing layer, resulting in decreasing photoresponse with increasing film thickness[18]. To circumvent these problems, we put forward an idea to replace β-FeSi$_2$ films with β-FeSi$_2$ NCs, which, as we suggested, can be epitaxially embedded into the silicon matrix due to enhanced elasticity, which is typical for nano-size materials. In our previous work we also demonstrated that a light-emitting silicon diode with embedded β-FeSi$_2$ NCs has a high-quality defect-free structure[19,20], so photogenerated carriers from β-FeSi$_2$ NCs move through the defect-free silicon layer. All of the abovementioned factors provide grounds for applying a silicon-silicide approach for the development of opto-couples.

This work follows the first study of photoelectrical properties of similar diode structures in open-circuit voltage mode[21] that was performed earlier by our group and in photocurrent mode at low temperature[22]. We showed the possibility of expanding the spectral sensitivity into the NIR region.

Results

Figure 1 shows a cross-sectional Transmission Electron Microscopy (TEM) image of the grown sample. A well-defined multilayered structure with β-FeSi$_2$ NCs was observed. The High Resolution Transmission Electron Microscopy (HRTEM) image denotes the existence of two types of NCs. The first type is the small NCs, several nanometres in diameter, with slightly elongated shape, which are located strictly at the depth of the Fe layer epitaxy. The first type dominates on the TEM images. The second type is spherical shape NCs, with a diameter of about 15–20 nm, occupying two or more layers. It is obvious that embedding of β-FeSi$_2$ NCs has not caused the formation of any significant defects in the silicon layers, despite the lattice mismatch between the materials. As a consequence, there are no mismatch dislocations at the heterointerface. It can be assumed that the absence of the linear defects resulted from the small size of the NCs. In this case it is possible to accumulate elastic deformation in NCs rather than change to a relaxed state accompanied by the generation of defects. This situation is quite similar to the pseudomorphic growth of the thin films.

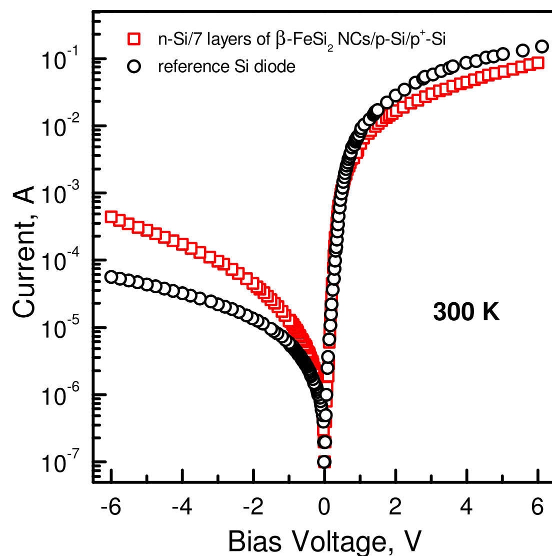

Figure 2. ***I-V*** **characteristics of Si/β-FeSi$_2$ NCs/Si and reference diode structures measured in the dark condition at room temperature.**

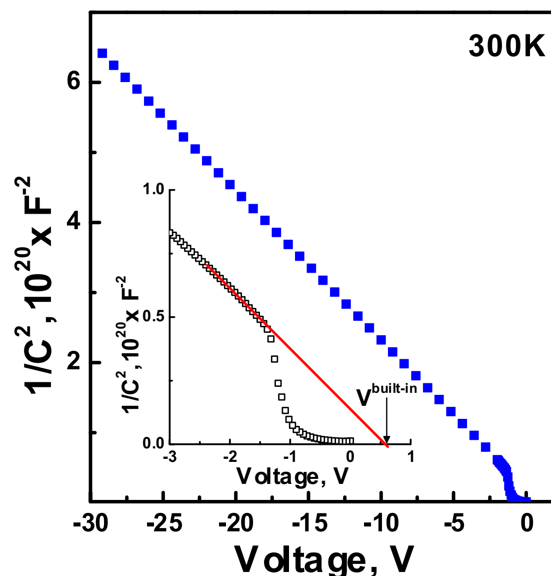

Figure 3. ***1/C^2-V*** **characteristic of Si/β-FeSi$_2$ NCs/Si photodiode structure measured in the dark condition at 300 K.** The intersection point of the red line with the voltage axis corresponds to the value of the built-in potential of the Si *p-n* junction at given doping levels and temperature.

Figure 2 shows the room temperature *I-V* characteristics of the Si/β-FeSi$_2$ NCs/Si photodiode structure and reference Si *p-n* diode. The diodes show good rectifying behaviour, as expected, for the conventional Si ones: the forward current is more than approximately two orders of magnitude greater than that under reverse bias. Estimated values of the series and shunt resistances are 42 Ω and 100 kΩ respectively for the photodiode structure containing β-FeSi$_2$ NCs, while in the case of the reference diode they are 30 Ω and 180 kΩ. Both diodes demonstrate nearly the same reverse saturation current of 0.11 μA and ideality factor of 1.

The dependencies of $1/C^2$ versus V (Fig. 3) showed that regardless of the presence of the NCs the value of built-in potential of the Si/β-FeSi$_2$ NCs/Si structure along with the reference diode is 0.54 eV, which is in good agreement with the value for a conventional Si *p-n* junction at room temperature, at the given doping levels of the Si substrate ($N_d = 5 \times 10^{14}$ cm^{-3}) and epitaxial *p*-Si layers ($N_a = 1 \times 10^{14}$ cm^{-3}). Furthermore, on the $1/C^2$ curve there is a linear part in the reverse bias range from −30 to −1 V, suggesting that it is due to the reduction of the interface state of the mesa diode[15]. From the foregoing, one can

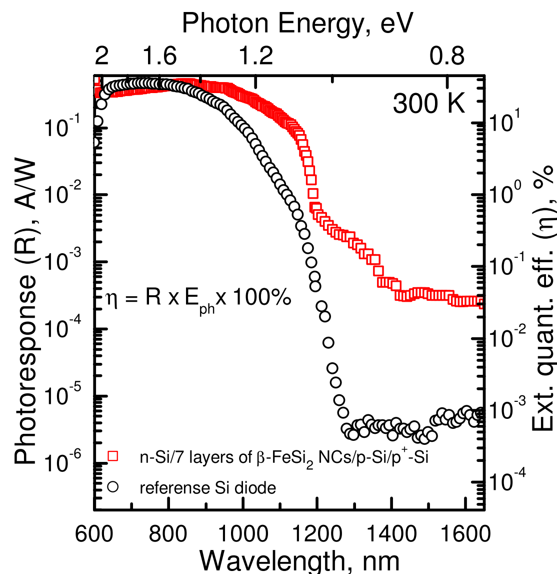

Figure 4. Photoresponse spectrum of the Si/β-FeSi$_2$ NCs/Si diode measured at room temperature under zero bias conditions (circles) and calculated spectrum of the external quantum efficiency in comparison with the reference Si *p-n* junction (squares).

conclude that embedding of β-FeSi$_2$ NCs into the depletion region of the Si *p-n* junction does not cause the formation of a significant amount of interface states.

At room temperature, the current under illumination is only slightly greater than the dark current, which can be associated with the relatively small amount of the β-FeSi$_2$ (seven layers with only 0.4 nm of Fe in each) in comparison with the β-FeSi$_2$ films on Si substrates, which show one order of magnitude difference between dark current and current under illumination[15,23–26]. On the other hand, embedded β-FeSi$_2$ NCs form mainly scattered layers (Fig. 1) in silicon matrix, with a surface density of 10^{11} cm^{-2} at most, as was shown in our previous works[20,27]. Thus, the part of the NIR light passes through the structure without photocarrier generation.

Measured photoresponse spectra of the structures at room temperature and zero bias are presented in Fig. 4. It is obvious that embedding of only seven layers of β-FeSi$_2$ NCs into the silicon *p-n* junction resulted in: (i) enhancement of the spectral range of photosensitivity up to 1600 nm (0.77 eV); (ii) the photoresponse (*R*) being enhanced by more than two orders of magnitude at the telecommunication wavelengths; (iii) an almost ten-fold increase in photoresponse close to the silicon absorption edge (1000–1200 nm) as a result of the contribution of β-FeSi$_2$ NCs.

Discussion

The Selected-Area Fast Fourier Transformation (SAFFT) was applied to analyse the phase composition of the sample. The SAFFT for the type I NCs (see Methods Section) reveals, besides the typical Si patterns, four pairs of spots corresponding to β-FeSi$_2$ planes with interplanar distances of 7.72 Å, 2.06 Å, 1.97 Å and 2.36 Å. These systems of planes are identified as (010) or (001) because of the large similarity between the b and c lattice constants of the β-FeSi$_2$, (201), (331), and (312), respectively. The angle between β-FeSi$_2$ (010)/(001) and Si (111) planes is 1.5°, suggesting almost coherent epitaxy with a corresponding epitaxy relationship or the formation of a low-angle boundary between the NCs and Si matrix.

The same measurements for the type II NCs represented in Fig. 1b (see the "Methods" section) confirmed that they correspond to β-FeSi$_2$ phase as well. There are three identified interplanar distances of 4.91 Å, 4.80 Å and 3.89 Å that are coincident to the (100), (111), and (010) or (001) planes, respectively. The angle between the β-FeSi$_2$ (100) and Si (110) planes is 3°. Thus, for the type II NCs, as well as for the small one, almost coherent epitaxy with the silicon matrix or low-angle boundary case takes place. The difference in the epitaxial relationships, in our opinion, is attributed to the difference in sizes of the NCs.

Based on the measured photoresponse, we estimated the spectral dependence of the external quantum efficiency (η) of our device and reference diode following Sze[28]. The device at zero bias conditions demonstrates a room temperature external quantum efficiency of near to 0.2% at 1300 nm (Fig. 4). The relatively low photocurrent can be explained if one takes into consideration the small amount of the material capable of absorbing NIR light, which results in NCs contributing poorly to the generation of photocarriers. That is why we had to use a structure similar to *n-i-p* in order to multiply carriers applying reverse bias, as the absorption of NIR light in β-FeSi$_2$ NCs would result in the generation of carriers which diffuse into the silicon, causing the development of an electron avalanche[29]. The existence of the avalanche process is also confirmed by an exponential growth of the photoresponse when the reverse

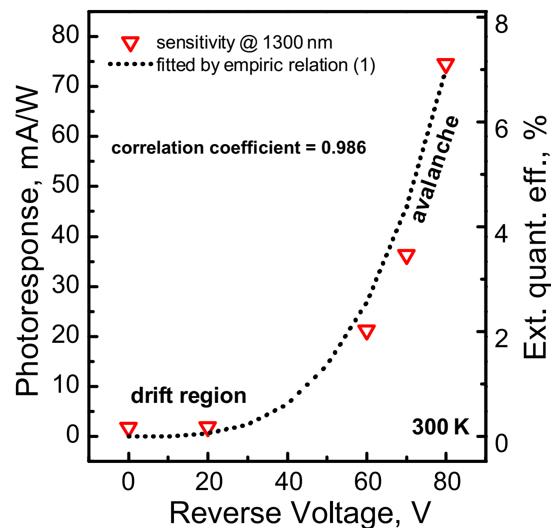

Figure 5. Experimental responsivity–reverse voltage dependence of the Si/β-$FeSi_2$ NCs/Si photodiode fitted by the empirical relation.

bias exceeds 50–60 volts (Fig. 5), which corresponds to the avalanche mode. According to Fig. 5, the reverse bias dependence of the photoresponse at 1300 nm is fitted well by the empirical relation[30] for the avalanche multiplication process:

$$R \propto \sqrt{V_b + V} \times \left(\frac{V}{V_{br}}\right)^n, \tag{1}$$

where V_b is the built-in voltage of the Si *p-n* junction, V_{br} is the breakdown voltage, and n is 3 for the *p*-type of the diode base[31]. The efficiency increases via avalanche multiplication in addition to the voltage root-square dependence of the *p-n* junction depletion layer. In our device we obtain a breakdown voltage of 54 V, a responsivity of 20 mA/W, and a value of the avalanche gain of 5. The maximum value of the external quantum efficiency obtained for the device is about 7%. From the analysis of the expression, it follows that: (i) the decrease of the breakdown voltage will result in a significant increase of the photoresponse, and (ii) it is possible to slightly increase the photoresponse by increasing the value of the built-in potential, which is restricted by the band gap of Si. The former can be achieved by changing the conduction type of the diode base to the *n*-type, which corresponds to $n = 5$ in the empirical expression[31]. In addition, a decrease in the thickness and dopant concentration of the Si layer (105 nm and $N_a = 1 \times 10^{14}\,cm^{-3}$ for the current device) reduces the breakdown voltage.

At room temperature, the photoresponse and external quantum efficiency values at the wavelength of 1300 nm in the avalanche mode ($R = 20$ mA/W; $\eta = 2\%$) are quite comparable with those of β-$FeSi_2$ thick films on Si ($R = 3$–15 mA/W; $\eta = 1$–2%)[23–26] and even exceed the values obtained for a β-$FeSi_2$ homojunction[32]. At the same time, we took advantage of the conventional Si *p-n* junction and expanded the functionality of the silicon diode structure in NIR photodetection, increasing the photoresponse by more than two orders of magnitude at important wavelengths for optical communications by adding a small amount of Fe to the initial system, while for the same results it is necessary to use films of β-$FeSi_2$ (90–100 nm of Fe)[23–26]. Moreover, it was shown that embedding of β-$FeSi_2$ NCs resulted in an increase of the sensitivity at the silicon absorption edge by more than one order of magnitude. It is interesting to note that the proposed approach gave rise to an increase in the integrated value of external quantum efficiency in the spectral range of 600–1700 nm from 18.7%, in the case of the reference Si photodiode, up to 23.3% for the p^+-Si/*p*-Si/β-$FeSi_2$ NCs/*n*-Si photodiode at zero bias. This fact suggests that embedding of β-$FeSi_2$ NCs into Si may also result in increasing performance of the conventional silicon solar cells.

To explain the gathering process of photogenerated carriers we propose a band diagrams of the diode structure in equilibrium and nonequilibrium states (Fig. 6). After the generation of carriers in the NCs, they diffuse into the *p*-type silicon layers, where the built-in potential of the Si *p-n* junction separates them. Then acceleration of the carriers by an external electric field takes place and the carriers may get sufficient energy for impact ionization of the silicon atoms, thereby developing an avalanche.

While constructing the band diagram in equilibrium state, we supposed that the applied bias drops entirely at the Si *p-n* junction rather than at the Si/β-$FeSi_2$ heterojunction. This assumption is confirmed by calculation of the relation between relative built-in voltages in each of the semiconductors expressed by the formula[33]:

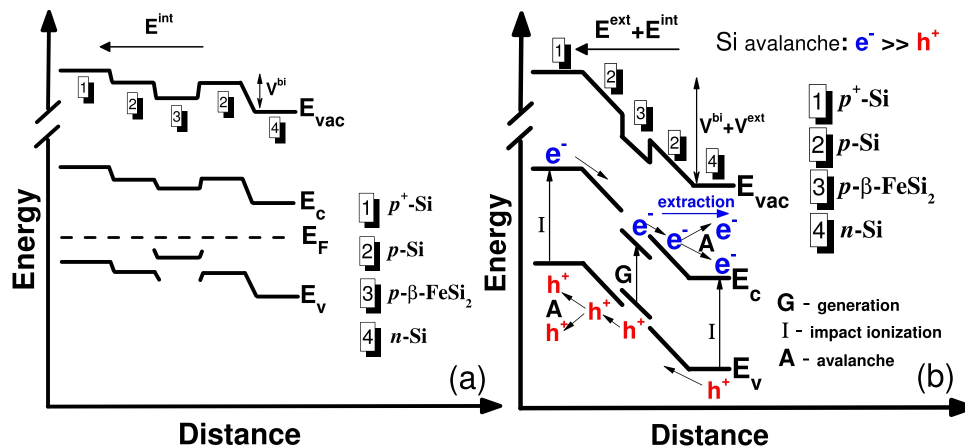

Figure 6. Band diagram of the Si/β-FeSi$_2$ NCs/Si diode structure in equilibrium and nonequilibrium states.

$$\frac{V^{\beta-FeSi2}}{V^{Si}} = \frac{N_{\alpha}^{Si} \times \varepsilon^{Si}}{N_{\alpha}^{\beta} \times \varepsilon^{\beta-FeSi2}}, \tag{2}$$

where V^i is the relative built-in voltage, $N_a{}^i$ is the concentration of the acceptors (10^{14} and $2–3 \times 10^{17}\,cm^{-3}$ for Si and β-FeSi$_2$, respectively), and ε^i is the dielectric constant of the materials (11.8 for Si[34] and 27.6 for β-FeSi$_2$[35]). We speculated that β-FeSi$_2$ NCs formed by SPE – as well as thin β-FeSi$_2$ films grown on Si in the same way – possess *p*-type conductivity with a carrier concentration of about $(2–3) \times 10^{17}\,cm^{-3}$[36]. Thus, the relation between relative built-in voltages is about 1 to 4000, suggesting that the applied bias drops at the Si *p-n* junction and does not cause a change in the energy level differences and barrier height at the β-FeSi$_2$/Si heterojunction in equilibrium state. The values of the work function of Si and β-FeSi$_2$ needed to construct the band diagram were taken from the literature data[34,37], and the Fermi level positions depending on temperature and doping level were calculated following Sze[27] using the value of the density of states in the valence band of *p*-type β-FeSi$_2$ obtained by Kasaya *et al.*[38].

Under the assumption of the low background photon flux at the zero bias voltage, following Keyes we calculated the Johnson-noise-limited specific detectivity (D^*), which limits the noise performance of the infrared photodiodes[39]. The obtained device specific detectivity at 300 K in zero bias conditions is $1.2 \times 10^9\,cm \times Hz^{1/2}/W$ at a wavelength of 1300 nm. The calculated value exceeds the results for β-FeSi$_2$ films on average[15,23,24] and is inferior in only in comparison with a passivated Si/β-FeSi$_2$ heterostructure[25].

Conclusion

In summary, we fabricated a Si/β-FeSi$_2$ NCs/Si photodiode structure grown by a combination of SPE for the formation of nanocrystallites with MBE for the epitaxy of the silicon capping layers. TEM investigations confirmed a well-defined multilayered structure with two types of embedded β-FeSi$_2$ NCs. SAFFT verified the presence of semiconducting β-phase. Depending on the type of NCs, either β-FeSi$_2$ (010)/(001) and Si (111) or β-FeSi$_2$ (100) and Si (110) epitaxy is observed with a misalignment angle of 3° at most, corresponding to the almost coherent or low-angle boundary case. Despite the lattice mismatch between materials, there are no mismatch dislocations at the heterointerface even in the case of type II β-FeSi$_2$ NCs.

I-V and *C-V* characteristics confirmed that embedding of the β-FeSi$_2$ NCs into the depletion region of the silicon photodiode does not substantially influence the diode rectifying properties, the reverse saturation current, or the formation of the additional significant concentration of trap centres resulting from the interface states or diffused iron atoms. We suppose that it is related to non-defect epitaxy and embedding of the small-sized NCs into the silicon matrix together with implementation of the SPE, which restricted iron diffusion to the silicon substrate to some extent and contained the formation of deep levels associated with it.

On the strength of the obtained results, we suppose that the fact that the values of photoresponse and external quantum efficiency of our device are comparable with those for β-FeSi$_2$ films is likely to be due to the defect-free heterointerfaces between the NCs and Si matrix, which results in a lower density of trap centres for photogenerated carriers and the advantages of avalanche multiplication.

Further improvements of our device may consist of the optimization of *p-n* junction parameters to operate at zero or small reverse biases. Another way to improve the performance, especially in the field of solar cells, is by embedding the NCs of different narrow band gap semiconducting silicides, for example

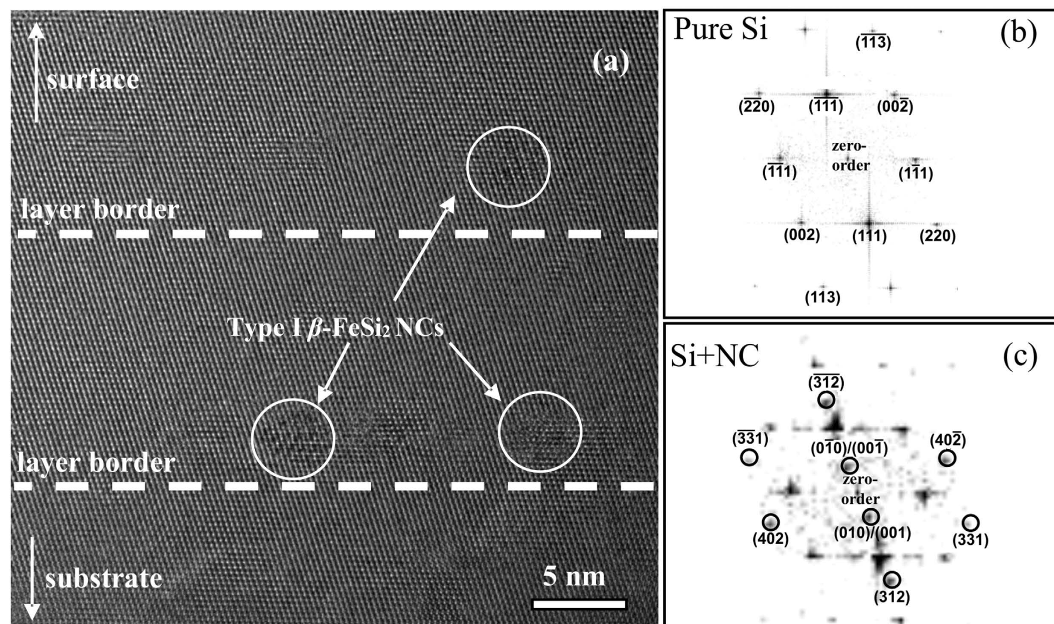

Figure 7. (**a**) HRTEM image of the Si/β-$FeSi_2$ NCs/Si structure showing type I β-$FeSi_2$ NCs, which are circled in white. Dashed lines indicate the borders of the layers. (**b**) SAFFT of the pure Si region. (**c**) SAFFT of the region containing β-$FeSi_2$ NC. All the reflexes differing from that of Si are circled in black and identified.

$CrSi_2$ (0.35–0.37 eV)[40,41] of Ca_3Si_4 (0.35–0.63 eV)[42], together with β-$FeSi_2$ to cover both the NIR and the short wave infrared region (1.4–3 μm) of the solar spectrum.

Methods

Sample growth. The sample was grown on *n*-type (7–10 Ω × cm) monocrystalline silicon substrate with (111) orientation. β-$FeSi_2$ NCs were formed by solid phase epitaxy (SPE) of 0.4 nm Fe at 630 °C followed by molecular beam epitaxy (MBE) of a thin (15 nm) weakly doped ($N_a = 1 \times 10^{14}\,cm^{-3}$) *p*-type Si layer at 750 °C. To obtain a multilayer structure, the SPE and MBE steps were repeated seven times, resulting in a total thickness of about 105 nm for the Si layer with embedded NCs (active region). The formation of the last covering layer was followed by the deposition of a p^+-type Si ($N_a = 10^{17}\,cm^{-3}$) layer (200 nm) at 750 °C to form an *n-i-p* structure, to some extent, and to achieve the ohmic contact with the Al contact layer. More detailed information about the growth procedure can be found in our previous works[20,21]. Next, the sample was chemically treated to form a mesa diode for photovoltaic measurements. Finally, Au-Sb alloy and Al were deposited to form contacts with *n*-Si and *p*-Si, respectively. For comparison, a similar diode structure was formed without NCs on the same substrate using the same deposition technique (referred to as the reference diode), with the only difference being in the thickness of the *p*-type epitaxial layer (600 nm).

Crystal structure analysis. The study of the structure and morphology of nanocrystallites was performed using a JEOL-4000EX electron microscope operated at 400 kV, which is characterized by a spatial resolution by points to point of 0.16 nm and by lines of 0.1 nm, and a TITAN 80–300 instrument equipped with a spherical aberration corrector of the objective lens and an electron beam monochromator and characterized by a spatial resolution of 0.08 nm. The (110) cross-sections for HRTEM studies were prepared in a standard manner by etching with argon ions. The Digital Micrograph software (GATAN) was used for digital processing of experimental HRTEM images.

Selected Area Fast Fourier Transforms. were performed using ImageJ software. The accuracy in determining the interplanar spacings was 0.05 nm, and calibration was carried out by well-known Si reflexes. Crystallographic planes were used as identifiers in all the SAFFT images; fold reflexes were not displayed in order to avoid cluttering the figures. Figures 7 and 8 show cross-sectional HRTEM images (a), SAFFT images of pure Si matrix (b), and SAFFT images of the type I and type II β-$FeSi_2$ NCs (c), respectively. When identifying reflexes, in addition to comparing the estimated interplanar distances, the angles between crystallographic planes, which are material independent, were checked for accordance. Therefore, we managed to eliminate from consideration other silicide phases such as Fe_3Si, ε-FeSi, α-$FeSi_2$, or γ-$FeSi_2$, which may have resulted in the presence of additional spots on the SAFFT images, which might be incorrectly taken as corresponding to β-$FeSi_2$.

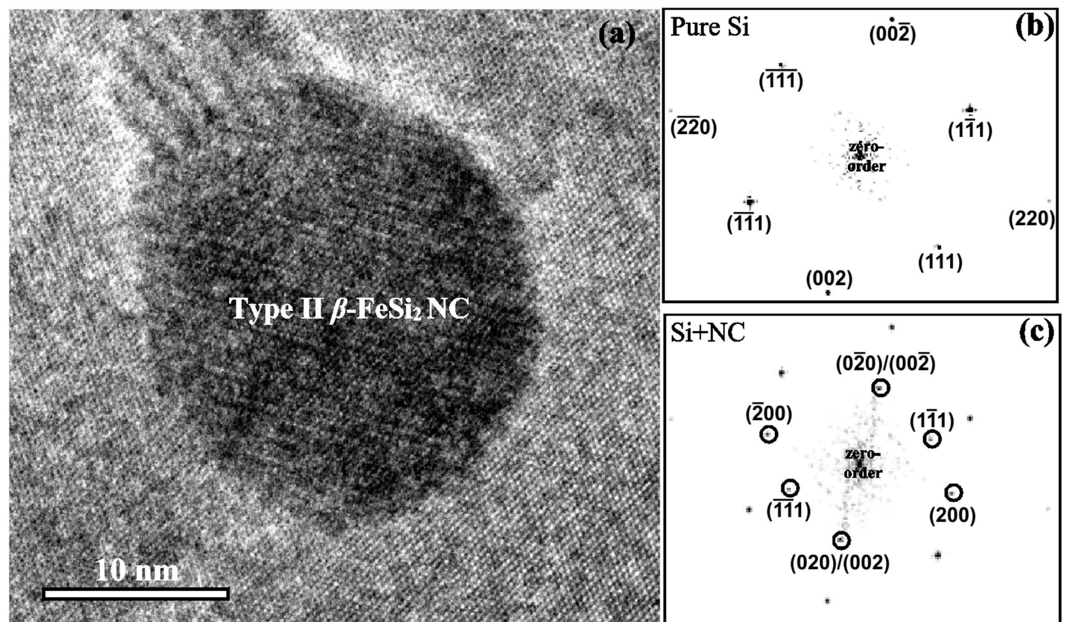

Figure 8. (**a**) HRTEM image of the Si/β-$FeSi_2$ NCs/Si structure showing type II β-$FeSi_2$ NC. (**b**) SAFFT of the pure Si region. (**c**) SAFFT for the region containing β-$FeSi_2$ NC. All the reflexes differing from that of Si are circled in black and identified.

Device characterization. Current-voltage (*I-V*) and capacitor-voltage (*C-V*) characteristics of the mesa diode were measured on an E7-20 immittance meter in the dark and under illumination conditions. Photoresponse measurements were carried out using a calibrated tungsten lump as a light source and a monochromator (Solar Tii, MS3504i) by the standard lock-in technique (Stanford Research Systems, DSP Lock-in amplifier SR830) with an optical chopper (f = 882 Hz). All the spectra were registered in a photocurrent mode.

References

1. Udono, H., Kikuma, I., Okuno, T., Masumoto, Y. & Tajima, H. Indirect optical absorption of single crystalline β-$FeSi_2$. *Appl. Phys. Lett.* **85,** 1937–1939 (2004).
2. Leo, Y.-F. *et al.* Wavelength-extended photovoltaic infrared photodetectors. *Appl. Phys. Lett.* **104,** 131101 (2014).
3. Hoang, A. M., Chen, G., Haddadi, A., Abdollahi Pour, S. & Razeghi, M. Demonstration of shortwavelength infrared photodiodes based on type-II InAs/GaSb/AlSb superlattices. *Appl. Phys. Lett.* **100,** 211101 (2012).
4. Tseng, H. H. *et al.* GeSn-based p-i-n photodiodes with strained active layer on a Si wafer *Appl. Phys. Lett.* **103,** 231907 (2013).
5. Oehme, M. *et al.* GeSn-on-Si normal incidence photodetectors with bandwidths more than 40 GHz. *Opt. Express* **22,** 839 (2014).
6. Wang, J. & Lee, S. Ge-photodetectors for Si-based optoelectronic integration. *Sensors.* **11,** 696 (2011).
7. Michel, J., Liu, J. & Kimerling, L. C. High-performance Ge-on-Si photodetectors. *Nat. Photonics* **4,** 527 (2010).
8. Kaschel, M., Schmid, M., Oehme, M., Werner, J. & Schulze, J. Germanium photodetectors on Silicon-on-insulator grown with differential molecular beam epitaxy in silicon wells. *Solid State Electron.* **60,** 105 (2011).
9. Gan, X. *et al.* Chip-integrated ultrafast graphene photodetector with high responsivity. *Nat. Photonics* **7,** 883 (2013).
10. Pospischil, A. *et al.* CMOS-compatible graphene photodetector covering all optical communication bands. *Nat. Photonics* **7,** 892 (2013).
11. Bost, M. C. & Mahan, J. A clarification of the index of refraction of beta-iron disilicide. *J. Appl. Phys.* **64,** 2034 (1988).
12. Suzuno, M., Koizumi, T. & Suemasu, T. *p*-Si/β-$FeSi_2$/*n*-Si double-heterostructure light-emitting diodes achieving 1.6 μm electroluminescence of 0.4 mW at room temperature. *Appl. Phys. Lett.* **94,** 213509 (2009).
13. Tatar, B., Kutlu, K. & Urgen, M. Synthesis of β-$FeSi_2$/Si heterojunctions for photovoltaic applications by unbalanced magnetron sputtering. *Thin Solid Films* **516,** 13 (2007).
14. Isobe, T., Nakashima, H. & Hashimoto, K. Diffusion coefficient of interstitial iron in silicon. *Jpn. J. Appl. Phys.* **28,** 1282 (1989).
15. Funasaki, S. *et al.* Fabrication of mesa structural *n*-type nanocrystalline-$FeSi_2$/*p*-type Si heterojunction photodiodes by liftoff technique combined with photolithography. *Phys. Status Solidi C* **10,** 1785 (2013).
16. Han, M., Tanaka, M., Takeguchi, M., Zhang, Q. & Furuya, K. High-resolution transmission electron microscopy study of interface structure and strain in epitaxial β-$FeSi_2$ on Si (111) substrate. *J. Cryst. Growth* **255,** 93 (2003).
17. Takarabe, K. *et al.* Optical properties of β-$FeSi_2$ under pressure. *Phys. Rev. B* **65,** 165215 (2002).
18. Shaban, M., Nakashima, K., Yokoyama, W. & Yoshitake, T. Photovoltaic properties of *n*-type β-$FeSi_2$/*p*-type Si heterojunctions. *Jpn. J. Appl. Phys.* **46,** L667 (2007).
19. Galkin, N. G. *et al.* Room temperature 1.5 μm light-emitting silicon diode with embedded β-$FeSi_2$ nanocrystallites. *Appl. Phys. Lett.* **101,** 163501 (2012).
20. Galkin, N. G., Chusovitin, E. A., Shamirsaev, T. S., Gutakovski, A. K. & Latyshev, A. V. Growth, structure and luminescence properties of multilayer Si/β-$FeSi_2$ NCs/Si/…/Si nanoheterostructures. *Thin Solid Films* **519,** 8480 (2011).
21. Goroshko, D. L. Enhancement of near IR sensitivity of silicon-silicide based photodetectors. *Phys. Status Solidi C* **10,** 1844 (2013).
22. Shevlyagin, A. V., Goroshko, D. L., Chusovitin, E. A., Galkin, K. N. & Galkin, N. G. Characterization of the silicon/β-$FeSi_2$ nanocrystallites heterostructures for the NIR photodetection at low temperature. *Jpn. J. Appl. Phys.* **54,** 07JB02 (2015).

23. Shaban, M., Nomoto, K., Izumi, S. & Yoshitake, T. Characterization of near-infrared *n*-type β-$FeSi_2$/*p*-type Si heterojunction photodiodes at room temperature. *Appl. Phys. Lett.* **94,** 222113 (2009).
24. Shaban, M., Izumi, S., Nomoto, K. & Yoshitake, T. *n*-type β-$FeSi_2$/intrinsic-Si/*p*-type Si heterojunction photodiodes for near-infrared light detection at room temperature. *Appl. Phys. Lett.* **95,** 162102 (2009).
25. Promos, N., Yamashita, K., Iwasaki, R. & Yoshitake, T. Effects of hydrogen passivation on near-infrared photodetection of *n*-type β-$FeSi_2$/*p*-type Si heterojunction photodiodes. *Jpn. J. Appl. Phys.* **51,** 108006 (2012).
26. Izumi, S., Shaban, M., Promos, N., Nomoto, K. & Yoshitake, T. Near-infrared photodetection of β-$FeSi_2$/Si heterojunction photodiodes at low temperatures. *Appl. Phys. Lett.* **102,** 032107 (2013).
27. Galkin, N. G., Goroshko, D. L., Chusovitin, E. A., Galkin, K. N. & Dotsenko, S. A. Silicon-silicide quasi-zero dimensional heterostructures for silicon based photonics, opto- and thermoelectronics. *Phys. Status Solidi C* **10,** 1670 (2013).
28. Sze, S. M. & Ng, K. K. *Physics of Semiconductor Devices* (John Wiley & Sons, inc. publications, New Jersey 2007).
29. Wegrzecka, I. *et al.* Design and properties of silicon avalanche photodiodes. *Opto-electron. Rev.* **12,** 95 (2004).
30. Desiatov, B., Goykhman, I., Shappir, J. & Levy, U. Defect-assisted sub-bandgap avalanche photodetection in interleaved carrier-depletion silicon waveguide for telecom band. *Appl. Phys. Lett.* **104,** 091105 (2014).
31. Staroselskiy, V. I. *Fizika poluprovodnikovih priborov mikroelektroniki* (Moscow 2009) (In Russian).
32. Liu, Z. *et al.* Doping of β-$FeSi_2$ films with boron and arsenic by sputtering and its application for optoelectronic devices. *Opt. Mater.* **27,** 942 (2005).
33. Sharma, B. L. & Purohit, R. K. *Semiconductor heterojunctions* (Pergamon Press, New York 1974).
34. Levinshtein, M., Rumyantsev, S. & Shur, M. *Handbook Series on Semiconductor Parameter* (World Scientific, 1996).
35. Landolt-Börnstein *Non-Tetrahedrally Bonded Binary Compounds II, Group III Condensed Matter* (Springer Berlin Heidelberg 2000).
36. Tassis, D. H. *et al.* Optical and electrical characterization of high quality β-$FeSi_2$ thin films grown by solid phase epitaxy. *Appl. Surf. Sci.* **102,** 178 (1996).
37. Fujimoto, H. *et al.* Photoemission study on the valence band of a β-$FeSi_2$ thin film using synchrotron radiation. *Dalton T*. **40,** 6023 (2011).
38. Kasaya, M. *et al.* Valence band density of states of the iron silicides studied by soft x-ray emission spectroscopy. *J. Phys. Soc. Jpn.* **63,** 4097 (1994).
39. Keyes R. J. *Optical and Infrared Detectors* (Springer, Berlin, 1977).
40. Bellani, V. *et al.* Theory and experiment on the optical properties of $CrSi_2$. *Phys. Rev. B* **46,** 9380 (1992).
41. Galkin, N. G., Maslov, A. M. & Konchenko, A. V. Optical and photospectral properties of $CrSi_2$ A-type epitaxial films on Si(111). *Thin Solid Films* **311,** 230 (1997).
42. Migas, D. B., Shaposhnikov, V. L., Filonov, A. B., Dorozhkin, N. N. & Borisenko, V. E. New semiconducting silicide Ca_3Si_4. *J. Phys.-Condens. Mat.* **19,** 346207 (2007).

Acknowledgements

This work has been carried out with financial support from the Russian Federation President's grant (No. MK-6343.2013.8). HRTEM studies were performed using the equipment of CCU "Nanostructures". Part of the work was carried out with the support of the Ministry of Education and Science of the Russian Federation (project ID RFMEFI62114X0004) and RSCF (project No. 14-22-00143).

Author Contributions

N.G. and E.A. planned and supervised the experiment. A.V. grew the sample in the ultrahigh-vacuum chamber. A.K. performed structural analysis on the electron microscopes. A.V. and D.L. analysed the transmission electron microscopy images and identified the nanocrystallites' crystal structure. E.A. formed the mesa structure based on the grown sample. A.V. and D.L. conducted *I-V*, *C-V*, and photoresponse measurements. N.G. and A.V. constructed the band diagram. K.N. calibrated and adjusted the optical system for electro-optical measurements. All the authors discussed the results and contributed to the refinement of the paper.

Additional Information

Competing financial interests: The authors declare no competing financial interests.

How to cite this article: Shevlyagin, A.V. *et al.* Enhancement of the Si *p-n* diode NIR photoresponse by embedding β-$FeSi_2$ nanocrystallites. *Sci. Rep.* **5**, 14795; doi: 10.1038/srep14795 (2015).

This work is licensed under a Creative Commons Attribution 4.0 International License. The images or other third party material in this article are included in the article's Creative Commons license, unless indicated otherwise in the credit line; if the material is not included under the Creative Commons license, users will need to obtain permission from the license holder to reproduce the material. To view a copy of this license, visit http://creativecommons.org/licenses/by/4.0/